Introduction

For several years *in vivo* and *in vitro*-based evidence has demonstrated the ability of amniotic membrane to provide a natural substrate upon which cells can grow[1-3]. Subsequently, human amniotic membrane (AM) is now firmly established as an important adjunct for ocular surface reconstruction across a broad spectrum of conditions[4] where it is often directly applied as a patch or a graft. For more serious conditions, such as limbal stem cell deficiency, AM taken from the fetal sac has also been employed as a substrate on to which donor corneal epithelial progenitor (limbal) cells are expanded, forming tissue engineered constructs suitable for surgical application[5]. However such therapeutic applications of AM often results in its post operative positioning within the visual field and sometimes, as in limbal stem cell transplantation, for prolonged or indefinite periods. In such cases the question of AM's transparency becomes crucial.

AM is the most structurally robust of the fetal membranes[6] consisting of a single layer of epithelial cells on a thick basement membrane which in turn lies upon layers of collagenous tissue interspersed with mesenchymal cells maintaining the mechanical integrity of the tissue[7]. Interstitial collagens (types I and III) predominate and form parallel bundles of collagen fibrils that produce a scaffold similar in ultrastructual organisation to that seen within the stroma of the cornea[8]. The AM stroma however is considerably thinner than that of the human cornea and, when used therapeutically, the amniotic epithelia are lost and replaced by native corneal epithelia[9]. However, AM stroma can persist in its native form for many months following transplantation under specific conditions[8].

Recently we have shown that there exists a significant variation in structure between different areas of the amniotic sac[10, 11] but despite the increasing use of AM in ophthalmic therapeutic applications there is presently little consideration given to the importance such variation in membrane structure may have on subsequent therapeutic effect, especially clinical transparency. Previously we have investigated the fine structural organisation of collagen fibrils within wounded and normal corneas and successfully related changes in fibril organisation to corneal transparency[12-19]. Thus, considering the previously observed similarities in structure between AM stroma and corneal stroma we have now applied our expertise in understanding corneal transparency to the transparency of clinically relevant AM.

Materials and methods

Collection and storage of human amniotic membrane

Following elective Caesarean section at term, unlinked anonymised samples of amniotic membrane were taken from fetal sac membranes adjoining, but not overlaying the placenta. Fetal membranes overlaying the placenta were not included as they are not commonly used in stem cell transplantation, the technique most strongly associated with the positioning of AM within the visual field for prolonged or indefinite periods. Fetal sac membranes from six patients were collected from the Department of Obstetrics and Gynaecology, Queens Medical Centre, Nottingham, UK, after full local ethics committee approval and in compliance with the Declaration of Helsinki. The fetal membranes were prepared in accordance with a previously published procedure[11]. Firstly, the chorion was separated manually from the amnion and discarded; the remaining AM washed with phosphate-buffered saline (PBS) containing antibiotics (5 ml of 0.5% levofloxacin) to remove blood. Persistent blood

stained AM edges were dissected away and not used. Then under sterile conditions samples (4 cm×4 cm) of AM were taken from areas adjacent to the placental disc (proximal amnion) and approximately 10 cm from the placental disc (distal amnion). These samples were chosen from areas of the AM which were coherent and translucent. The dissected AM samples were stored at −80°C in PBS. These samples were thawed before further examination and subsequently termed freeze-thawed AM. It has previously been confirmed that there is no difference between fresh and frozen AM in terms of clinical efficacy[20].

Four further placentas, providing samples for freeze dried AM, were received either as a gift (Dr T. Nakamura, Kyoto Prefectural University of Medicine, Japan having been prepared according to their published method[21]) or supplied commercially (Acelagraft, Celgene Cellular Therapeutics, NJ).

Transmission measurements.

The freeze-thawed amniotic samples were incubated in Dispase (Gibco) at 37°C for 2 hours and the epithelium removed by scrapping. Both the freeze-thawed and freeze dried samples were incubated in PBS at room temperature for 2 hours before the transmission of light through each sample was measured. Each sample of AM in PBS was flattened and held securely between the two glass plates of a 35mm slide mount. The glass slide mount maintained the AM in a hydrated state with no wrinkles or air bubbles. Each mounted sample was then placed, in turn, within a spectrophotometer (PYE Unicom, SP8-100) and percent transmission was recorded through the visible spectrum (400 – 700 nm). The process was repeated three times for each sample, each time exposing a different area of tissue to the incident light beam. The transmission values were zeroed by subtracting the glass slide mount with PBS alone.

Refractive index measurements.

Following transmission measurements, the refractive index of each AM sample was quantified using a bench-top Abbe 60 Series Refractometer (Bellingham and Stanley Ltd., Tunbridge Wells, England). The refractive index was measured from three different areas of each sample independently by two observers and the average value calculated.

Thickness measurements.

Immediately following transmission measurements a small area (10mm^2) from each sample was embedded in Tissue Tek (Fisher Scientific, UK), snap frozen in liquid nitrogen and stored at -80°C. Cryo-sections (7μm) were then stained with haematoxylin and eosin and thickness measurements across the AM recorded using a calibrated microscope with digital camera (Zeiss, Axioskop 2). To compensate for the natural heterogeneity of AM structure three serial sections were taken from three regions of increasing depth through each embedded sample, ten measurements were taken from each section and the results averaged.

Predicted transparency calculations.

Transparency through corneal stroma can be predicted using an established model, the direct summation of fields for light scattering by fibrils[12, 22, 23]. In this study we applied the same model to predict transparency through corneal stroma with a thickness artificially reduced to that of AM. This facilitated a direct comparison in transmission spectra between the cornea (predicted) and AM (actual) by normalising for tissue thickness. Briefly, assuming there is no absorption, the fraction of light

transmitted undeviated through the cornea is related to the total scattering cross-section per fibril per unit length, σ, by the equation:

$$F(\lambda) = e^{-\rho\sigma t} \quad \text{(Eq 1)}$$

where t is the thickness of the stroma, ρ is the bulk number density of fibrils in the stroma, and σ, the scattering cross-section, is a function of the following, 1) the size of the fibrils 2) the packing of the fibrils, 3) the refractive indices of the hydrated fibrils and hydrated interfibrillar matrix and, 4) wavelength (λ). t was calculated from our light microscopy measurements of AM, the size and packing of corneal collagen fibrils were taken from representative published electron micrographs of human corneal stroma[24] and the refractive index of the fibrils and interfibrillar matrix was taken from previously published data[25].

Results

Light microscopy confirmed that the epithelial cells had been successfully removed from the freeze-thawed AM and that none were present on the surface of freeze-dried AM prior to transmission measurements (Figure 1). The freeze-dried, freeze-thawed distal and freeze-thawed proximal AM had a mean thickness of 21.6μm (sd ± 5.6), 64.3 (sd ± 20.9) and 95.3μm (sd ± 27.9) respectively. The freeze-dried AM was significantly thinner than the freeze-thawed AM ($p < 0.01$, Student's t-Test). Within the freeze-thawed AM samples thickness was significantly greater in areas proximal to the placenta when compared to AM collected from areas distal to the placenta ($p < 0.01$, Student's t-Test) (Figure 2).

Transparency (percent transmission of visible light) differed significantly between the three types of AM investigated (freeze-dried, freeze-thawed proximal and freeze-thawed distal). Transparency increased in line with tissue thickness, the freeze-dried AM (thinnest) having the highest transmission spectra and the freeze-thawed proximal AM (thickest) having the lowest transmission spectra (Figure 3).

The freeze-dried, freeze-thawed distal and freeze-thawed proximal AM had a mean refractive index of 1.335 (sd ± 0.001), 1.334 (sd ± 0.002) and 1.357 (sd ± 0.002) respectively. There was no significant difference between the refractive index of freeze-dried and freeze-thawed distal AM both having a similar refractive index to water (1.333). The refractive index of freeze-thawed proximal AM was significantly higher than the freeze-thawed distal AM ($p < 0.001$, Student's t-Test) and much nearer to the refractive index of the corneal stroma (1.375)[25] (Figure 4).

The direct summation of fields method facilitated a comparison in transparency between corneal tissue of different thicknesses (Figure 5). The values of the thicknesses used were taken from the AM thickness measurements by light microscopy (Figure 2). By comparing the predicted levels of transparency with the actual AM transmission spectra, shown in figure 3, freeze-dried, freeze-thawed distal and freeze-thawed proximal AM were calculated to be 85%, 83% and 68% as transparent as the human cornea respectively once normalised for stromal thickness.

Discussion

The results suggest that significant variations in the optical properties of AM exist. We have shown that preservation and sampling protocol can influence both the transmission of visible light and refractive index of AM used for ocular surface regeneration. The divergence in measured transparency between freeze-dried AM and

freeze-thawed AM, despite having a similar refractive index, is most likely explained by differences in tissue thickness since when normalised for thickness there was very little difference between the subsequent predicted corneal transparencies. However, the relative smoothness of the freeze-dried AM surface and complete absence of epithelial cells would have also reduced the scatter of incident light increasing its transparency.

Interestingly the smallest relative difference in refractive index between human cornea and AM was shown by the freeze-thawed proximal sample. This may have some clinical relevance as the larger the difference in refractive index between cornea and transplanted AM the greater the chance of scatter at the interface between the two tissues would be. If this were the case and despite its lower transparency, freeze-thawed proximal AM may be more suitable for the packing of deep corneal wounds, such as ulcers, especially if we consider that AM can persist unaltered within the corneal stroma for 12 months[8].

Using AM for ocular surface reconstruction within the visual field, tissue taken from an area of the amniotic sac distal to the placenta offers the most transparency. However, freeze dried AM preservation provides an increased level of transparency over a freeze-thaw method of preservation.

Acknowledgements

We would like to acknowledge funding support from the NC3R, Diawa Anglo-Japanese Foundation and JSPS Furusato Award (CJC). KMM is a Royal Society/Wolfson Foundation Merit Award holder.

Competing interest: None declared

Figure legends

Figure 1. Freeze-dried AM lacks the presence of epithelial or stromal cells and is of uniform thickness (A). Freeze-thawed AM is uneven in its thickness, AM collected distal to the placental (B) is thinner than AM collected proximal/adjacent to the placenta (C). Whilst epithelial cells have been successfully removed by enzyme treatment followed by scraping, stromal cells persist (arrows). However these cells are likely to be devitalised following the freeze-thaw process. Scale bars = 20μm.

Figure 2. Thickness measurements of freeze-dried, freeze-thawed distal and freeze-thawed proximal AM were taken from the light micrographs. Proximal AM was significantly found to be the thickest whilst freeze-dried AM was found to be significantly the thinnest. Error bars correspond to standard error.

Figure 3. The percentage transmission of visible light was compared through freeze-dried, freeze-thawed distal and freeze-thawed proximal AM. The freeze-thawed proximal AM has the lowest transmission spectra whereas the freeze-dried had the highest. Error bars correspond to standard error.

Figure 4. Refractive index was compared between freeze-dried, freeze-thawed distal and freeze-thawed proximal AM. No significant difference was observed between freeze-dried and freeze-thawed distal AM, both similar to water. Freeze-thawed proximal AM had a significantly high refractive index than the other types of AM. *The refractive index values of human cornea and water were taken from published data[25]. Error bars correspond to standard error.

Figure 5. Predicted transmission of visible light through cornea at various thicknesses using the direct summation of fields method. The graph clearly shows a decrease in transparency with increasing tissue thickness. Thickness values correspond to the measured thickness of freeze-dried, freeze-thawed distal and freeze-thawed proximal AM. A comparison between these spectra and measured spectra through AM (Figure 3.) facilitates a direct evaluation of transparency between cornea and AM by normalising for tissue thickness.

References

1. Meller D, Pires RT, Tseng SC. Ex vivo preservation and expansion of human limbal epithelial stem cells on amniotic membrane cultures. Br J Ophthalmol 2002;86:463-71.
2. Schwab IR. Cultured corneal epithelia for ocular surface disease. Trans Am Ophthalmol Soc 1999;97:891-986.
3. Koizumi N, Inatomi T, Quantock AJ, Fullwood NJ, Dota A, Kinoshita S. Amniotic membrane as a substrate for cultivating limbal corneal epithelial cells for autologous transplantation in rabbits. Cornea 2000;19:65-71.
4. Gomes JA, Romano A, Santos MS, Dua HS. Amniotic membrane use in ophthalmology. Curr Opin Ophthalmol 2005;16:233-40.
5. Tsai RJ, Li LM, Chen JK. Reconstruction of damaged corneas by transplantation of autologous limbal epithelial cells. N Engl J Med 2000;343:86-93.
6. Moore RM, Mansour JM, Redline RW, Mercer BM, Moore JJ. The Physiology of Fetal Membrane Rupture: Insight Gained from the Determination of Physical Properties. Placenta 2006;In Press, Corrected Proof.
7. Malak TM, Ockleford CD, Bell SC, Dalgleish R, Bright N, Macvicar J. Confocal immunofluorescence localization of collagen types I, III, IV, V and VI and their ultrastructural organization in term human fetal membranes. Placenta 1993;14:385-406.
8. Connon CJ, Nakamura T, Quantock AJ, Kinoshita S. The Persistence of Transplanted Amniotic Membrane in Corneal Stroma. American Journal of Ophthalmology 2006;141:190-192.
9. Nubile M, Dua HS, Lanzini TE-M, et al. Amniotic membrane transplantation for the management of corneal epithelial defects: an in vivo confocal microscopic study. Br J Ophthalmol 2008;92:54-60.
10. Connon CJ, Nakamura T, Hopkinson A, et al. The biomechanics of amnion rupture: an x-ray diffraction study. PLoS ONE 2007;2:e1147.

11. Hopkinson A, McIntosh RS, Tighe PJ, James DK, Dua HS. Amniotic Membrane for Ocular Surface Reconstruction: Donor Variations and the Effect of Handling on TGF-{beta} Content. Invest. Ophthalmol. Vis. Sci. 2006;47:4316-4322.
12. Connon CJ, Marshall J, Patmore AL, Brahma A, Meek KM. Persistent haze and disorganization of anterior stromal collagen appear unrelated following phototherapeutic keratectomy. J Refract Surg 2003;19:323-32.
13. Connon CJ, Meek KM. Organization of corneal collagen fibrils during the healing of trephined wounds in rabbits. Wound Repair Regen 2003;11:71-8.
14. Meek K, Leonard D, Connon C, Dennis S, Khan S. Transparency, swelling and scarring in the corneal stroma. Eye 2003;17:927-36.
15. Connon CJ, Meek KM. The structure and swelling of corneal scar tissue in penetrating full-thickness wounds. Cornea 2004;23:165-71.
16. Connon CJ, Meek KM, Kinoshita S, Quantock AJ. Spatial and temporal alterations in the collagen fibrillar array during the onset of transparency in the avian cornea. Exp Eye Res 2004;78:909-15.
17. Meek KM, Elliott GF, Sayers Z, Whitburn SB, Koch MH. Interpretation of the meridional x-ray diffraction pattern from collagen fibrils in corneal stroma. J Mol Biol 1981;149:477-88.
18. Meek KM, Leonard DW. Ultrastructure of the corneal stroma: a comparative study. Biophys J 1993;64:273-80.
19. Meek KM, Quantock AJ. The use of X-ray scattering techniques to determine corneal ultrastructure. Prog Retin Eye Res 2001;20:95-137.
20. Adds PJ, Hunt CJ, Dart JKG. Amniotic membrane grafts, "fresh" or frozen? A clinical and in vitro comparison. Br J Ophthalmol 2001;85:905-907.
21. Nakamura T, Yoshitani M, Rigby H, et al. Sterilized, freeze-dried amniotic membrane: a useful substrate for ocular surface reconstruction. Invest Ophthalmol Vis Sci 2004;45:93-9.
22. Freund DE, McCally RL, Farrell RA. Direct summation of fields for light scattering by fibrils with applications to normal corneas. Appl Opt 1986;25:2739.
23. McCally RL, Freund DE, Zorn A, et al. Light-scattering and ultrastructure of healed penetrating corneal wounds. Invest Ophthalmol Vis Sci 2007;48:157-65.
24. Komai Y, Ushiki T. The three-dimensional organization of collagen fibrils in the human cornea and sclera. Invest Ophthalmol Vis Sci 1991;32:2244-58.
25. Leonard DW, Meek KM. Refractive indices of the collagen fibrils and extrafibrillar material of the corneal stroma. Biophys J 1997;72:1382-7.

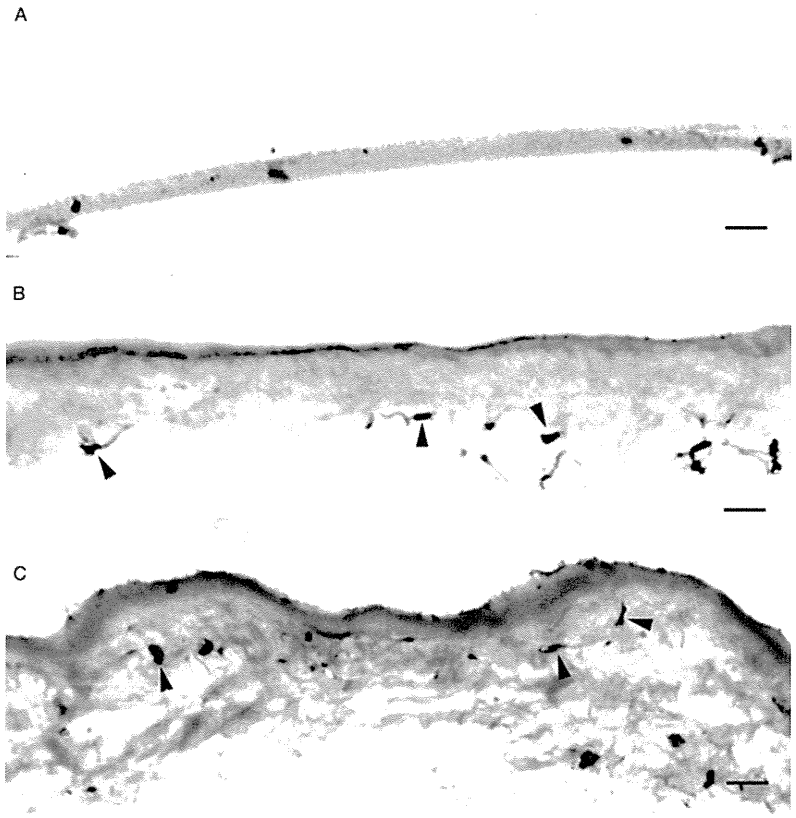

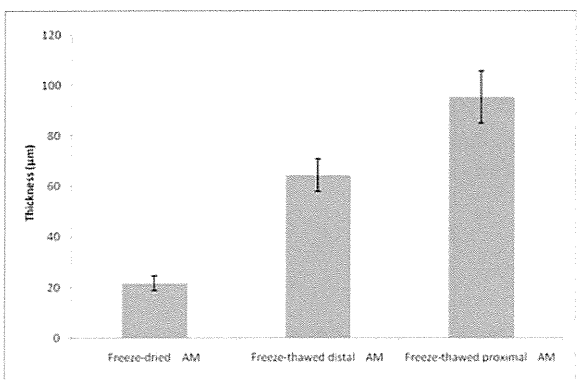

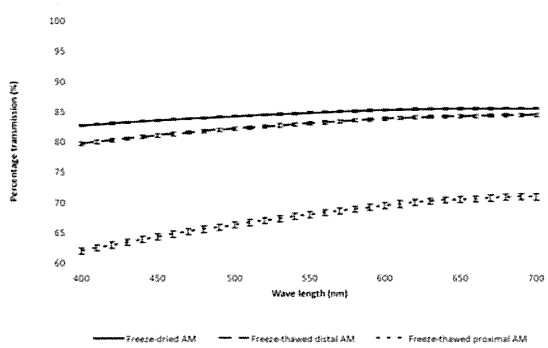

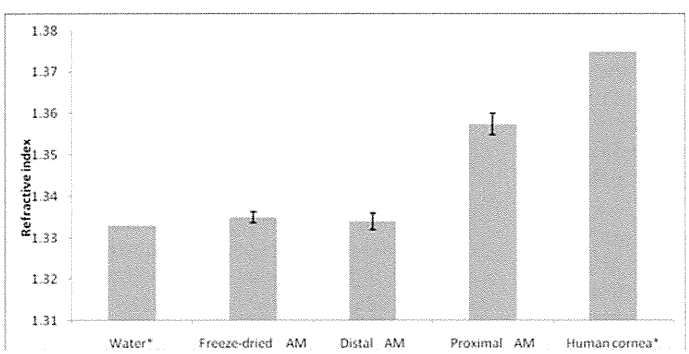

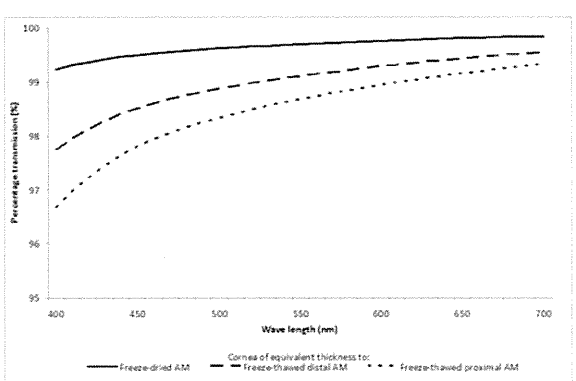

Functional Role of Thymic Stromal Lymphopoietin in Chronic Allergic Keratoconjunctivitis

Akira Matsuda,[1,2] *Nobuyuki Ebihara,*[1] *Norihiko Yokoi,*[2] *Satoshi Kawasaki,*[2] *Hidetoshi Tanioka,*[2] *Tsutomu Inatomi,*[2] *Rene de Waal Malefyt,*[3] *Junji Hamuro,*[2] *Shigeru Kinoshita,*[2] *and Akira Murakami*[1]

Purpose. Previous reports have shown that thymic stromal lymphopoietin (TSLP) plays a role in atopic diseases. This study was undertaken to investigate the expression of TSLP in the giant papillae obtained from patients with vernal keratoconjunctivitis (VKC) or atopic keratoconjunctivitis (AKC), and its functional roles were analyzed.

Methods. TSLP mRNA expression was examined in resected conjunctival samples obtained from four patients with VKC/AKC and three control subjects by reverse transcription-polymerase chain reaction. Anti-TSLP, anti-dendritic cell-limbic system-associated membrane protein (anti-DC-LAMP), and anti-tryptase immunohistochemical staining was performed with 10 resected giant papillae. Human conjunctival epithelial (HCJE) cells were stimulated with poly I:C, with and without endosomal inhibitor, to examine TSLP mRNA expression. Cultured human mast cells were stimulated with recombinant (r)TSLP to analyze the downstream effect of TSLP.

Results. All four VKC/AKC samples showed TSLP mRNA expression; however, no TSLP mRNA expression was found in the control conjunctivae. Anti-TSLP immunohistochemical staining showed preferential expression in the epithelial cells and some infiltrated cells of the giant papillae, but not in the control conjunctivae. Double immunohistochemical staining with TSLP and DC-LAMP or tryptase showed the existence of activated dendritic cells and mast cells near TSLP-positive cells in the giant papillae. Real-time PCR analysis showed that poly I:C induced TSLP mRNA expression in HCJEs in an endosomal-function-dependent manner and that rTSLP could induce IL-13 mRNA expression in the mast cells synergistically with IL-33.

Conclusions. The TSLP protein produced in conjunctival epithelial cells plays a role in severe ocular allergy through the activation of dendritic cells and mast cells in synergy with other cytokines. (*Invest Ophthalmol Vis Sci.* 2010;51:151-155) DOI:10.1167/iovs.09-4183

From the [1]Department of Ophthalmology, Juntendo University School of Medicine, Tokyo, Japan; the [2]Department of Ophthalmology, Kyoto Prefectural University of Medicine, Kyoto, Japan; and the [3]Department of Immunology, Schering-Plough Biopharma, Palo Alto, California.

Supported by Grants-in-Aid 19659454 (SK) and 18604009 and 21592239 (AM) from MEXT (Ministry of Education, Culture, Sports, Science, and Technology) Japan.

Submitted for publication June 19, 2009; revised August 7, 2009; accepted August 11, 2009.

Disclosure: **A. Matsuda**, None; **N. Ebihara**, None; **N. Yokoi**, None; **S. Kawasaki**, None; **H. Tanioka**, None; **T. Inatomi**, None; **R. de Waal Malefyt**, Schering-Plough Biopharma (E); **J. Hamuro**, None; **S. Kinoshita**, None; **A. Murakami**, None

Corresponding author: Akira Matsuda, Department of Ophthalmology, Juntendo University School of Medicine, 2-1-1, Hongo, Bunkyo-Ku, Tokyo, 113-8431, Japan; akimatsu@juntendo.ac.jp.

Both vernal keratoconjunctivitis (VKC)[1] and atopic keratoconjunctivitis (AKC)[2] are types of severe chronic allergic conjunctivitis in which giant papillae formation is frequently observed. In the acute stage, there is massive local infiltration by mast cells, T helper 2 (Th2) cells, and eosinophils, and there is Th2 cytokine expression. Recently, the roles of thymic stromal lymphopoietin (TSLP), an IL-7-like cytokine, were investigated in atopic diseases (e.g., atopic dermatitis and atopic asthma) because of its specific expression in the epithelium in the presence of atopic diseases and its ability to activate $CD11c^+$ dendritic cells (DCs), resulting in Th2 cell priming by the DCs.[3,4] In this study, we examined the expression of TSLP mRNA and protein using in vivo samples obtained from the resected giant papillae for therapeutic purposes. We also examined the existence of activated DCs by immunohistochemical methods.

On the other hand, it has been reported that proinflammatory stimuli including synthetic double-strand RNA (poly I:C) could induce TSLP expression in various epithelial cells, including bronchial epithelial cells,[5] keratinocytes,[6] and corneal epithelial cells.[7] Stimulation with poly I:C, which is considered to be mimicking the viral infection cascade, has some clinical relevance, because other studies have reported that children who have had respiratory syncytial virus (RSV) infection are more likely to develop bronchial asthma with IgE production.[8,9] Therefore, we evaluated the effect of poly I:C-mediated signals of TSLP mRNA induction, using the human conjunctival epithelial (HCJE) cell line,[10] and tried to inhibit poly I:C-induced TSLP expression using the endosomal inhibitor bafilomycin A for the purpose of possible therapeutic intervention. In addition, we examined the downstream effect of TSLP in human cultured mast cells in synergy with another Th2 cytokine, IL-33,[11,12] to elucidate the possible role of TSLP in the pathophysiology of severe chronic allergic conjunctivitis.

Material and Methods

Giant Papillae and Control Conjunctivae Samples

Giant papillae were resected for therapeutic purposes from four patients, three with AKC and one with VKC, and control conjunctivae tissue was biopsied from patients with cataract, pterygium, or melanoma during surgery after written informed consent was obtained for TSLP mRNA analysis (Table 1). Additional giant papillae samples were obtained from six patients with AKC and four with VKC for TSLP immunostaining analysis (Table 2). All procedures were approved by the ethics committees of Juntendo University School of Medicine and Kyoto Prefectural University of Medicine, and the study was conducted in accordance with the tenets of the Declaration of Helsinki. AKC was defined as a bilateral chronic inflammation of the conjunctiva and lids associated with atopic dermatitis, and VKC was defined as a chronic, bilateral, conjunctival inflammatory condition found in individuals predisposed by their atopic background; detailed information about pa-

TABLE 1. Clinical Information for RT PCR Analysis

Sample No.	Sex	Age	Diagnosis	Total IgE
1	M	21	AKC	4263
2	M	18	AKC	5218
3	M	12	VKC	92
4	M	32	AKC	1983
5	F	72	Cataract	ND
6	M	52	Pterygium	ND

tient selection was described elsewhere.[13] Upper bulbar conjunctivae resected from six patients with conjunctivochalasis were used as control samples, as previously described,[13] after informed consent was obtained (Table 3).

Antibodies, Reagents, and Cell Lines

We purchased mouse anti-DC-LAMP (CD208) monoclonal antibody from Beckman Coulter Japan (Tokyo, Japan), mouse anti-human tryptase antibody from Dako Japan (Kyoto, Japan), and Alexa-488-conjugated donkey anti-rat IgG and Alexa-594-conjugated donkey anti-mouse IgG antibodies from Invitrogen Japan (Tokyo, Japan). Rat anti-human TSLP monoclonal antibody was prepared as previously described.[4] HCJE was kindly provided by Ilene K. Gipson (Schepens Eye Research Institute, Philadelphia, PA) and maintained with defined keratinocyte serum-free medium (KSFM; Invitrogen Japan). The human mast cell line LAD2 was kindly provided by Arnold Kirshenbaum (National Institutes of Health, Bethesda, MD), and maintained as previously described.[14] Recombinant human (r)TSLP and recombinant human (r)IL-33 were obtained from Peprotech (London, UK), poly I:C was obtained from InvivoGen (San Diego, CA), and bafilomycin A1 was obtained from Sigma-Aldrich (St. Louis, MO).

Reverse-Transcription–Polymerase Chain Reaction

Total RNA was extracted from the giant papillae tissue (NucleoSpin II RNA isolation kit; Macherey-Nagel GmbH & Co., Duren, Germany), and cDNAs were prepared from 1 μg of total RNA by using random primers and reverse transcriptase (Superscript II; Invitrogen) according to the manufacturer's protocol. PCR primers for TSLP amplification were 5′-aacaagtgtcacaattacaag-3′ (forward) and 5′-aatgtcccttagaaaagtatg-3′ (reverse), which are designed for amplifying the common region of TSLP transcript variants 1 and 2 (GenBank accession numbers: NM_033035.4 and NM_138551.3, respectively; 849-bp length; http://www.ncbi.nlm.nih.gov/Genbank; provided in the public domain by the National Center for Biotechnology Information, Bethesda, MD). PCR reaction was performed as follows: initial denaturation at 94°C for 5 minutes and at 94°C for 1 minute, annealing at 60°C for 1 minute, and extension at 72°C for 1 minute (35 cycles). IL-4[15] and IL-13[16] amplification was performed according to previously published methods, with the following pairs of primers: IL-4: 5′-ctcacagagcagaagactctgtg-caccgag-3′(forward), and 5′-cacaggacaggaattcaagcccgccaggcc-3′ (reverse); and IL-13: 5′-ccacggtcattgctctctcacttgcc-3′ (forward), 5′-ccttgt-gcgggcagaatccgctca-3′ (reverse).

TABLE 3. Summary of TSLP Immunostaining of Control Conjunctivae

Sample No.	Age	Sex	Diagnosis	TSLP	
				Epithelium	Substantia propria
1	70	F	Conjunctivochalasis	−	−
2	65	M	Conjunctivochalasis	−	−
3	71	F	Conjunctivochalasis	−	−
4	74	M	Conjunctivochalasis	−	−
5	53	F	Conjunctivochalasis	−	−
6	75	F	Conjunctivochalasis	−	−

−, negative immunostaining.

Immunohistochemistry

Giant papillae were frozen in OCT compound, and cryostat sections were then cut, mounted on slides, and fixed in 4% paraformaldehyde in PBS. Nonspecific staining was blocked (30 minutes) with blocking buffer (10% normal donkey serum, 1% bovine serum albumin [BSA] in PBS). Anti-TSLP monoclonal antibody (10 μg/mL) was then applied and reacted overnight at 4°C. After they were washed with PBS, the slides were incubated for 30 minutes with Alexa 488-conjugated anti-rat IgG. Double immunohistochemical staining was performed with pairs of anti-TSLP and anti-tryptase antibodies and anti-TSLP and anti-CD208 antibodies. The pair of primary antibodies was applied to the samples simultaneously, and the secondary antibodies (Alexa 488 anti-rat IgG and Alexa and 594 anti-mouse IgG antibodies) were then applied after the samples were washed with PBS.

HCJE Stimulation with Poly I:C and the Effect of Bafilomycin A for Poly I:C Stimulation

HCJE cells were grown in 12-well dishes and used in the subconfluent state. Poly I:C (5 μg/mL) was added to HCJE cells and incubated for 1, 3, and 8 hours in a CO_2 incubator. Simultaneously, 10 nM bafilomycin A was added to some wells to inhibit endosomal functions in the HCJE cells.

Mast Cell Stimulation with rTSLP/rIL-33 and Downstream Signal Analysis

LAD2 cells (2×10^4 cells per well in a 24-well dish) were stimulated with rTSLP (10 ng/mL) for 1, 3, and 16 hours. rIL-33 (10 ng/mL) was

TABLE 2. Summary of TSLP Immunostaining of Giant Papillae

Sample No.	Age	Sex	Total IgE	Specific IgE	Diagnosis	TSLP	
						Epithelium	Substantia Propria
1	16	F	509	positive	VKC	++	+
2	22	M	89	positive	VKC	+	+
3	13	M	2319	positive	VKC	++	++
4	18	M	375	positive	AKC	+	+
5	17	M	17260	positive	AKC	+	++
6	21	M	1904	positive	AKC	+	+
7	16	M	3763	positive	AKC	+/−	+
8	19	M	124	negative	VKC	+/−	+
9	34	M	22800	positive	AKC	+	++
10	45	F	28	negative	AKC	+	+

++, prominent immunostaining; +, positive immunostaining; +/−, sporadic immunostaining.

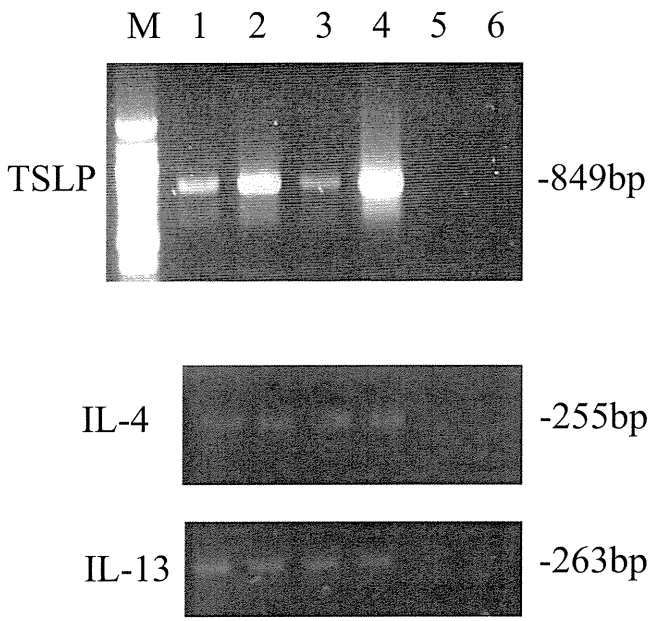

FIGURE 1. RT-PCR analysis of TSLP, IL-4, and IL-13 mRNA expression in human conjunctival tissue. RT-PCR was performed with cDNA prepared from giant papillae (*lanes1-4*) and control conjunctivae (*lanes 5, 6*). M, DNA size markers. Single bands were observed at the predicted length (849 bp for TSLP, 255 bp for IL-4, and 263 bp for IL-13) of the PCR products (*lanes 1-4*).

added alone or simultaneously to LAD2 cells. IL-13 mRNA expression in LAD2 cells was quantified by real-time PCR.

Real-Time PCR Analysis of TSLP and IL-33 mRNA Expression

Total RNA was extracted from HCJE and LAD2 cells and cDNAs were prepared from 1 μg of total RNA by using random primers as just described. We used real-time PCR probes (*Taq*Man; Applied Biosystems [ABI], Foster City, CA) and primers specific for human TSLP (Hs01572934_g1), human IL-13 (Hs00174379_m1), and 18SrRNA (Assay-on-Demand gene expression products; ABI). Real-time PCR analysis was performed on a sequence-detection system (Prism 7300; ABI). The expression of TSLP in the HCJE cells was quantified by the standard curve method, by using 18SrRNA expression in the same cDNA as a control. We calculated a standard curve with full-length human TSLP cDNA obtained by PCR reaction and subcloned into pCRII dual promoter plasmid (Invitrogen). For IL-13 mRNA expression, the comparative Ct method was used, which utilizes 18SrRNA expression in the same cDNA as a control.

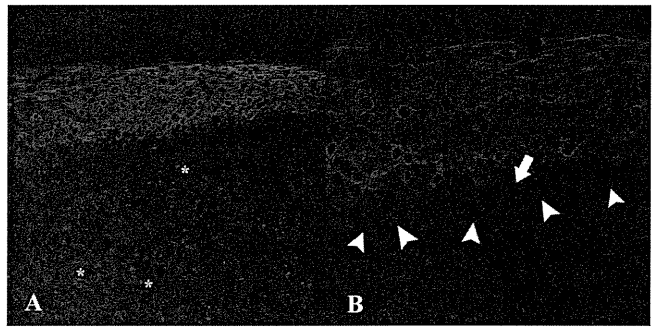

FIGURE 3. TSLP/tryptase double-immunohistochemical staining of giant papillae. Positive TSLP staining (*green*) was observed in the suprabasal-apical layers of conjunctival epithelium (**A**). Tryptase-positive mast cells (*red*) were observed underneath the epithelium, a few mast cells are also positive for TSLP (✱). (**B**) Tryptase-positive mast cells were observed around the basal cell layer of the epithelium (*arrow*) and beneath the epithelium. *Arrowheads*: the boundary between the epithelium and substantia propria. Original magnification: (**A**) ×200; (**B**) ×400.

RESULTS

RT-PCR Analysis of Giant Papillae Obtained from Patients with VKC/AKC

Total RNA was extracted from the giant papillae and control conjunctivae tissue, then RT-PCR was performed. TSLP mRNA expression was detected for all the giant papillae samples (Fig. 1, lanes 1-4); however, no TSLP mRNA expression was detected for control samples (Fig. 1, lanes 5-7).

Immunohistochemical Localization of TSLP

Anti-TSLP immunohistochemical staining was performed using giant papillae obtained from AKC/VKC patients as well as control conjunctivae. The epithelium of giant papillae showed cytoplasmic-positive immunostaining for TSLP protein (Fig. 2A). There was a clear boundary between the TSLP-positive and -negative epithelium (Fig. 2A). Additional positive TSLP staining was observed in some infiltrating cells in the giant papillae samples (Fig. 2A and 2B, asterisks). DC-LAMP-positive, activated dendritic cells were observed beneath the TSLP-positive epithelial cells and near the TSLP-positive cells in the substantia propria (Fig. 2A, arrowheads). No TSLP immunostaining was observed in the control conjunctiva sample (Fig. 2C). Double-immunostaining with anti-TSLP and anti-tryptase antibodies revealed that tryptase-positive mast cells were located beneath the TSLP-positive epithelium (Fig. 3), and some of the mast cells were found within and under the epithelium

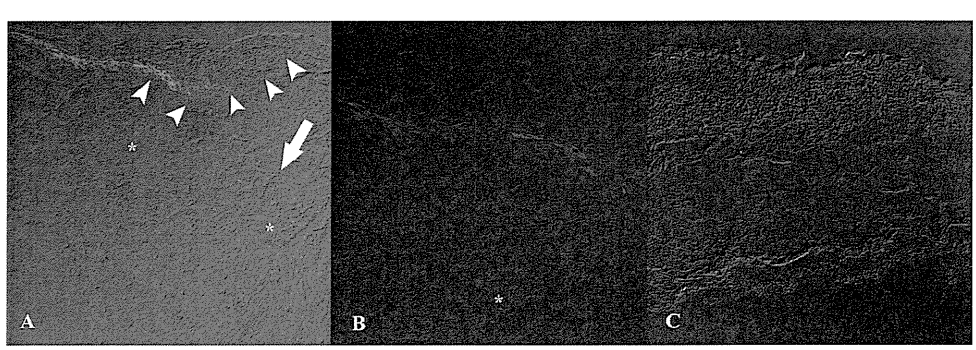

FIGURE 2. TSLP/DC-LAMP double-immunohistochemical staining of giant papillae. Cytoplasmic TSLP immunostaining (*green*) was observed in the epithelial cells of giant papillae. There is a clear boundary between the TSLP-positive- and -negative epithelium within the same section. The boundary between the epithelium and substantia propria is indicated by *arrowheads* (**A**, higher magnification in **B**). Some TSLP-positive cells were also observed at the substantia propria (*arrow*). DC-LAMP-immunopositive dendritic cells (*red*) were observed underneath the TSLP-positive conjunctival epithelium and near the TSLP-positive cells in the substantia propria (✱). No TSLP-positive staining was observed in the control conjunctiva (**C**). Original magnification: (**A**, **C**) ×200, (**B**) ×400.

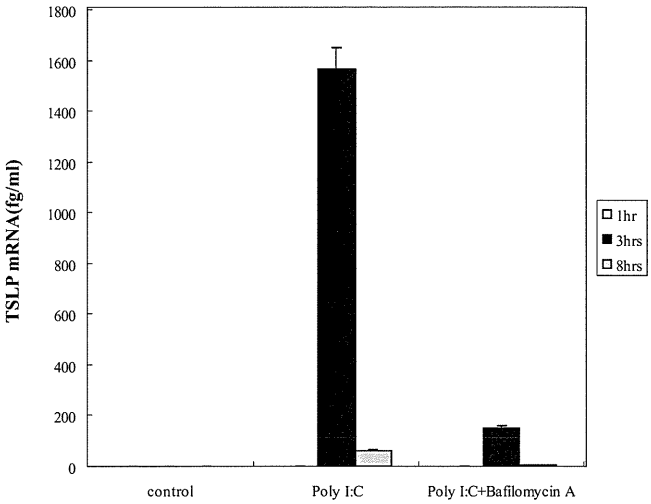

FIGURE 4. Real-time PCR analysis of TSLP mRNA expression using HCJE cells. The cells were stimulated with poly I:C (5 μg/mL) for 1, 3, and 8 hours, with or without the endosomal inhibitor bafilomycin A. cDNA was prepared from each sample, and TSLP mRNA expression was quantified by real-time PCR, with the standard curve method. Data are representative of results in three independent experiments performed in triplicate.

(Fig. 3B). A few mast cells were also positive for TSLP immunostaining (Fig. 3A, asterisks). The immunostaining results are summarized in Tables 2 and 3.

Poly I:C-Induced TSLP Expression in HCJE Cells

cDNAs were synthesized from total RNA isolated from poly I:C-stimulated HCJE cells. TSLP mRNA induction was observed in HCJE cells stimulated with poly I:C (5 μg/mL) at 3 hours after stimulation (Fig. 4). Simultaneous addition of 10 nM bafilomycin A showed inhibition of poly I:C-induced TSLP mRNA expression (Fig. 4).

TSLP-Induced IL-33 mRNA Expression in Synergy with IL-33

The human mast cell line LAD2 was stimulated with rTSLP (10 ng/mL), rIL-33 (10 ng/mL), and rTSLP+rIL-33 for 1, 3, and 16 hours. Relative IL-13 mRNA expression was quantified with real-time PCR. rTSLP alone did not induce IL-13 mRNA expression, and rIL-33 induced modest IL-13 expression (30-fold, compared with the unstimulated LAD2 cells). Co-stimulation of LAD2 cells with rTSLP and rIL-33 synergistically induced IL-13mRNA expression (150-fold) and peaked at 1 hour after co-stimulation (Fig. 5).

DISCUSSION

In this study, we detected in vivo expression of TSLP mRNA/protein in the giant papillae tissues obtained from patients with VKC/AKC, and no TSLP expression was observed in the control samples (Figs. 1, 2A, 2C). To the best of our knowledge, this is the first report of TSLP expression in an ocular surface disorder. As has been reported about other allergic diseases such as atopic dermatitis[4] and bronchial asthma,[17] preferential TSLP expression was observed in the epithelial cells of chronic allergic conjunctivitis. Restricted TSLP protein expression was clearly observed at the surface epithelial cells (Fig. 2A). This finding was also consistent with those in a previous report on atopic dermatitis.[4]

We also observed some TSLP-positive cells in the substantia propria of the giant papillae (Fig. 2, arrow). Corrigan et al.[18] recently reported that TSLP-positive neutrophils, mast cells, and macrophages were observed in the antigen-challenged dermis obtained from atopic patients. Therefore, we theorize that the TSLP-positive cells in the giant papillae may be these inflammatory cells. We found that at least some mast cells express TSLP protein (Fig. 3A, asterisks), which is consistent with previous studies that showed that the mast cells activated through the IgE receptor express TSLP mRNA.[4,19] Our double-immunohistochemistry results also showed that tryptase-positive mast cells localize in the vicinity of TSLP-positive epithelial cells in the giant papillae (Fig. 3B, arrow), and our result adds support to the proposal of Miyata et al.[20] that mast cells are essential for TSLP expression in the epithelium of the mouse allergic rhinitis model.

It is known that one of the major functions of TSLP is activating dendritic cells, which prime naïve T cells to produce the proallergic cytokines, such as IL-4, -5, and -13.[4] We therefore determined the existence of activated dendritic cells by using the dendritic cell activation marker DC-LAMP and found the existence of activated dendritic cells in the vicinity of the TSLP-positive cells (Fig. 2, asterisks). The DC-LAMP-positive dendritic cells were observed not only underneath the TSLP-positive epithelial cells but also near the TSLP-positive cells in the substantia propria (Fig. 2A, arrow). This result adds support to the recent results of Corrigan at al.,[18] who proposed a possible role of TSLP-positive inflammatory cells in the activation of dendritic cells in the dermis of atopic skin challenged with allergen.

As a next step, we examined the expression of TSLP mRNA in HCJE cells[10] with added poly I:C. As reported previously in bronchial epithelial cells[5] and corneal epithelial cells,[7] poly I:C stimulation induces TSLP mRNA expression in the conjunctival epithelial cells. We analyzed the time course of TSLP mRNA expression and found that it peaked at 3 hours after poly I:C stimulation (Fig. 4). Our results are consistent with those of Ma et al.,[7] who showed peak TSLP mRNA expression at 3 hours after stimulation of human corneal epithelial cells. We then tried to inhibit poly I:C-induced TSLP mRNA expression by the endosomal inhibitor bafilomycin. Previous reports showed that poly I:C-induced IL-6 expression in a peripheral blood mononuclear cell (PBMC) requires an acidic pH (pH5.7-6.5), and bafilomycin A could inhibit poly I:C-induced IL-6 expression by inhibiting the endosomal proton pump.[21] Our results showed that a 10 nM bafilomycin treatment blocked TSLP mRNA ex-

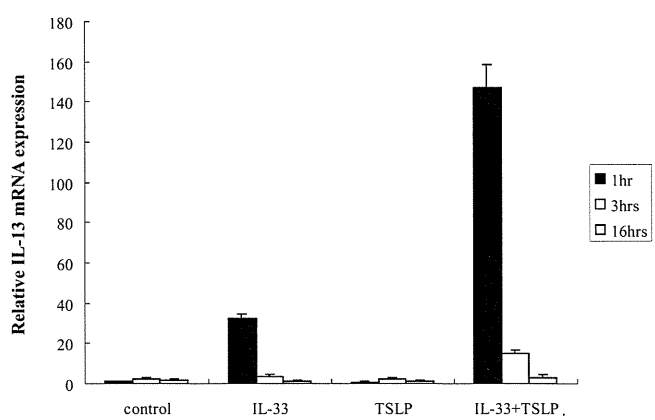

FIGURE 5. TSLP and IL-33 synergistically induced IL-13 expression in human mast cells (LAD2). The cells were stimulated with rTSLP (10 ng/mL), rIL-33 (10 ng/mL), and rTSLP+rIL-33 for 1, 3, and 16 hours. Relative IL-13 mRNA was shown to be comparable to that of unstimulated LAD2 cells obtained 1 hour after stimulation. Data are representative of results in three independent experiments performed in triplicate.

pression induced by 3-hour poly I:C stimulation (Fig. 4). We theorize that drugs that raise endosomal pH may be useful for inhibiting poly I:C-mediated TSLP expression. It is known that bafilomycin A is too toxic for clinical use; therefore, omeprazole, a proton pump inhibitor, or chloroquine, a competing basic compound that raises endosomal pH, which are widely used in the treatment of gastric ulcer and malaria, respectively, may be useful for this purpose.[22]

Finally, we examined the possible effector cells for TSLP in the chronic allergic conjunctivitis. Mast cells have been reported as one of the effector cells in TSLP signaling.[23] A previous report showed that the coculture of skin fragments from patients with atopic dermatitis (AD) with human mast cells induces TSLP protein expression and that anti-TSLP antibody treatment suppresses TSLP expression.[23] However, the authors did not perform direct stimulation of human mast cells with recombinant (r)TSLP. Therefore, we stimulated human mast cells with rTSLP and found that rTSLP treatment alone induced a minimum of IL-13 mRNA induction. A surprising finding showed that co-stimulation with another epithelial cell-derived Th2 cytokine, IL-33, had a synergistic effect for IL-13 mRNA expression in LAD2 cells (Fig. 5). In their study, Allakhverdi et al.[23] showed partial suppression of IL-13 expression using anti-TSLP antibody in a mast cell-lesional, AD-skin coculture model, so it is reasonable to consider that other skin-derived factor(s) also contribute to IL-13 mRNA expression. Very recently, we reported IL-33 protein expression in the epithelial cells of giant papillae as well as TSLP,[12] and so we considered that TSLP-IL-33 co-stimulation may play a role in the pathogenesis of chronic allergic diseases through the activation of mast cells.

In summary, we found in vivo expression of TSLP in the epithelial cells of giant papillae, and we theorize that TSLP protein may play a role in the pathogenesis of severe chronic allergic conjunctivitis through the activation of dendritic cells or mast cells in synergy with other proinflammatory cytokines such as IL-33. The double-stranded RNA molecule, associated with viral infection, may induce expression of TSLP, and the endosomal inhibitor bafilomycin may be useful for inhibiting this activation.

Acknowledgments

The authors thank Hisako Hitora-Takeshita for excellent technical support; Julian M. Hopkin for his invaluable continuous support; Ilene K. Gipson for providing the HCJE cell line; Arnold Kirshenbaum for providing the LAD2 cell line; and John Bush for editing the English.

References

1. Montan PG, Biberfeld PJ, Scheynius A. IgE, IgE receptors, and other immunocytochemical markers in atopic and nonatopic patients with vernal keratoconjunctivitis. *Ophthalmology.* 1995;102:725–732.
2. Foster CS, Rice BA, Dutt JE. Immunopathology of atopic keratoconjunctivitis. *Ophthalmology.* 1991;98:1190–1196.
3. Zhou B, Comeau MR, De Smedt T, et al. Thymic stromal lymphopoietin as a key initiator of allergic airway inflammation in mice. *Nat Immunol.* 2005;6:1047–1053.
4. Soumelis V, Reche PA, Kanzler H, et al. Human epithelial cells trigger dendritic cell mediated allergic inflammation by producing TSLP. *Nat Immunol.* 2002;3:673–680.
5. Kato A, Favoreto S Jr, Avila PC, Schleimer RP. TLR3- and Th2 cytokine-dependent production of thymic stromal lymphopoietin in human airway epithelial cells. *J Immunol.* 2007;179:1080–1087.
6. Kinoshita H, Takai T, Le TA, et al. Cytokine milieu modulates release of thymic stromal lymphopoietin from human keratinocytes stimulated with double-stranded RNA. *J Allergy Clin Immunol.* 2009;123:179–186.
7. Ma P, Bian F, Wang Z, et al. Human corneal epithelium-derived thymic stromal lymphopoietin: a potential link between the innate and adaptive immune responses via Toll-like receptors and Th2 cytokines. *Invest Ophthalmol Vis Sci.* 2009;50(6):2702–2709.
8. Welliver RC, Kaul TN, Ogra PL. The appearance of cell-bound IgE in respiratory-tract epithelium after respiratory-syncytial-virus infection. *N Engl J Med.* 1980;303:1198–1202.
9. Chen CH, Lin YT, Yang YH, et al. Ribavirin for respiratory syncytial virus bronchiolitis reduced the risk of asthma and allergen sensitization. *Pediatr Allergy Immunol.* 2008;19:166–172.
10. Gipson IK, Spurr-Michaud S, Argueso P, Tisdale A, Ng TF, Russo CL. Mucin gene expression in immortalized human corneal-limbal and conjunctival epithelial cell lines. *Invest Ophthalmol Vis Sci.* 2003;44:2496–2506.
11. Schmitz J, Owyang A, Oldham E, et al. IL-33, an interleukin-1-like cytokine that signals via the IL-1 receptor-related protein ST2 and induces T helper type 2-associated cytokines. *Immunity.* 2005;23:479–490.
12. Matsuda A, Okayama Y, Terai N, et al. The role of interleukin-33 in chronic allergic conjunctivitis. *Invest Ophthalmol Vis Sci.* Published online May 20, 2009.
13. Matsuda A, Okayama Y, Ebihara N, et al. Hyperexpression of the high-affinity IgE receptor-beta chain in chronic allergic keratoconjunctivitis. *Invest Ophthalmol Vis Sci.* 2009;50:2871–2877.
14. Kirshenbaum AS, Akin C, Wu Y, et al. Characterization of novel stem cell factor responsive human mast cell lines LAD 1 and 2 established from a patient with mast cell sarcoma/leukemia; activation following aggregation of FcepsilonRI or FcgammaRI. *Leuk Res.* 2003;27:677–682.
15. Goodman RE, Nestle F, Naidu YM, et al. Keratinocyte-derived T cell costimulation induces preferential production of IL-2 and IL-4 but not IFN-gamma. *J Immunol.* 1994;152:5189–5198.
16. Burd PR, Thompson WC, Max EE, Mills FC. Activated mast cells produce interleukin 13. *J Exp Med.* 1995;181:1373–1380.
17. Ying S, O'Connor B, Ratoff J, et al. Expression and cellular provenance of thymic stromal lymphopoietin and chemokines in patients with severe asthma and chronic obstructive pulmonary disease. *J Immunol.* 2008;181:2790–2798.
18. Corrigan CJ, Jayaratnam A, Wang Y, et al. Early production of thymic stromal lymphopoietin precedes infiltration of dendritic cells expressing its receptor in allergen-induced late phase cutaneous responses in atopic subjects. *Allergy.* 2009;64(7):1014–22.
19. Okayama Y, Okumura S, Sagara H, et al. FcepsilonRI-mediated thymic stromal lymphopoietin production by IL-4-primed human mast cells. *Eur Respir J.* 2009;34(2):425–35.
20. Miyata M, Hatsushika K, Ando T, et al. Mast cell regulation of epithelial TSLP expression plays an important role in the development of allergic rhinitis. *Eur J Immunol.* 2008;38:1487–1492.
21. de Bouteiller O, Merck E, Hasan UA, et al. Recognition of double-stranded RNA by human toll-like receptor 3 and downstream receptor signaling requires multimerization and an acidic pH. *J Biol Chem.* 2005;280:38133–38145.
22. Lee CM, Tannock IF. Inhibition of endosomal sequestration of basic anticancer drugs: influence on cytotoxicity and tissue penetration. *Br J Cancer.* 2006;94:863–869.
23. Allakhverdi Z, Comeau MR, Jessup HK, et al. Thymic stromal lymphopoietin is released by human epithelial cells in response to microbes, trauma, or inflammation and potently activates mast cells. *J Exp Med.* 2007;204:253–258.

Original article

Association between prostaglandin E receptor 3 polymorphisms and Stevens-Johnson syndrome identified by means of a genome-wide association study

Mayumi Ueta, MD, PhD,[a,c]* Chie Sotozono, MD, PhD,[a]* Masakazu Nakano, PhD,[b] Takazumi Taniguchi, PhD,[b] Tomohito Yagi, MD, PhD,[b] Yuichi Tokuda,[b] Masahiro Fuwa,[b] Tsutomu Inatomi, MD, PhD,[a] Norihiko Yokoi, MD, PhD,[a] Kei Tashiro, MD, PhD,[b] and Shigeru Kinoshita, MD, PhD[a] *Kyoto, Japan*

Background: Stevens-Johnson syndrome (SJS) and its severe variant, toxic epidermal necrolysis (TEN), are acute inflammatory vesiculobullous reactions of the skin and mucosa. They often affect the ocular surface and can result in permanent visual dysfunction.

Objectives: We sought to discover genetic markers for SJS/TEN susceptibility.

Methods: We performed a genome-wide association study with 60 patients and 300 control subjects. We applied stringent filter and visual assessments for selecting single nucleotide polymorphisms (SNPs) and a high false discovery rate threshold. We fine-mapped the region where a candidate SNP was found and confirmed the results by means of sequencing. We evaluated the function of agonist-activated prostaglandin E receptor 3 (EP3), the gene for which contained several SNPs, in regulating cytokine production in human conjunctival epithelial (CE) cells. The expression levels of EP3 in the CE cells from patients and control subjects were also compared.

Results: We identified 3 SNPs that passed the false discovery rate threshold. One (rs17131450) was close to the *EP3* gene. Therefore we analyzed the *EP3* region in detail and identified 5 other SNPs. We confirmed the association between SJS/TEN and all 6 SNPs. Activated EP3 was expressed in control CE cells, and it suppressed polyI:C-stimulated cytokine production, suggesting that EP3 might help prevent ocular surface inflammation. Concordantly, the EP3 levels were much lower in the CE cells of the patients than in those of the control subjects.

Conclusion: We demonstrated, using both genetic and functional analyses, that *EP3* could be a key player in the pathogenesis of SJS/TEN accompanied by ocular complications. (J Allergy Clin Immunol 2010;■■■:■■■-■■■.)

Key words: *Prostaglandin E receptor 3, Stevens-Johnson syndrome, toxic epidermal necrolysis, genome-wide association study, single nucleotide polymorphism*

Stevens-Johnson syndrome (SJS) and its severe variant, toxic epidermal necrolysis (TEN), are acute-onset mucocutaneous diseases (Fig 1, *A*) induced by infectious agents or an adverse reaction to a drug.[1-8] Although the annual incidences of SJS and TEN are very low, 0.4 to 1 and 1 to 6 cases per million persons, respectively,[8] they have a significant public health effect because the mortality rate is high (ie, 3% and 27%, respectively). Healthy children and adults can suddenly get these diseases, and any drug approved worldwide is a candidate instigator.[3,9-12] Associations between HLA type and drug-induced severe cutaneous adverse reactions, including SJS and TEN, have been reported.[13-21]

Patients with ocular involvement (50% to 68%)[8,11] exhibit severe conjunctivitis, and corneal epithelial defects often persist because of ocular surface inflammation.[4,22] Even after the skin lesions have healed, ocular surface complications, such as conjunctival invasion of the cornea, severe dryness of the eye, and, in some instances, keratinization of the ocular surface, can persist (Fig 1, *B*).[23] Representative causative drugs of SJS/TEN with ocular involvement are cold remedies, antibiotics, and nonsteroidal anti-inflammatory drugs (NSAIDs).[4,5,7,23] In this study we focused exclusively on patients with SJS/TEN with ocular involvement. Hereafter, "SJS/TEN" denotes SJS/TEN accompanied by ocular complications.

Although the pathobiological mechanisms underlying the onset of SJS/TEN have not been fully established, the extreme rarity of the cutaneous, mucosal, and ocular surface reactions to drug therapies led us to suspect individual susceptibility. Previously, we performed a single nucleotide polymorphism (SNP) association analysis of candidate genes to investigate whether a genetic predisposition for SJS/TEN exists and to identify culpable polymorphisms. We found SJS/TEN-associated polymorphisms in the genes encoding Toll-like receptor 3 (TLR3),[5-7] IL-4 receptor,[24,25] and Fas ligand[26] in ethnic Japanese patients. We also showed that in Japanese patients HLA-A*0206 is strongly associated with the disease.[27,28] Therefore it is quite obvious that not

From the Departments of [a]Ophthalmology and [b]Genomic Medical Sciences, Kyoto Prefectural University of Medicine, Kyoto, and [c]the Research Center for Inflammation and Regenerative Medicine, Faculty of Life and Medical Sciences, Doshisha University, Kyoto.

*These authors contributed equally to this work.

Supported in part by grants-in-aid for scientific research from the Japanese Ministry of Health, Labour and Welfare; the Japanese Ministry of Education, Culture, Sports, Science and Technology; a research grant from the Kyoto Foundation for the Promotion of Medical Science; and the Intramural Research Fund of Kyoto Prefectural University of Medicine.

Disclosure of potential conflict of interest: The authors have declared that they have no conflict of interest.

Received for publication March 2, 2010; revised July 24, 2010; accepted for publication August 5, 2010.

Reprint requests: Shigeru Kinoshita, MD, PhD, Department of Ophthalmology, Kyoto Prefectural University of Medicine, Hirokoji, Kawaramachi, Kamigyoku, Kyoto 602-0841, Japan. E-mail: shigeruk@koto.kpu-m.ac.jp.

0091-6749/$36.00

doi:10.1016/j.jaci.2010.08.007

Abbreviations used
BRLMM: Bayesian Robust Linear Model with a Mahalanobis distance classifier
CE: Conjunctival epithelium
EP3: Prostaglandin E receptor 3
FDR: False discovery rate
GAPDH: Glyceradlehyde-3-phosphate dehydrogenase
GWAS: Genome-wide association study
HapMap-CHB: HapMap Han Chinese
HapMap-JPT: HapMap Japanese
LD: Linkage disequilibrium
MAF: Minor allele frequency
NSAID: Nonsteroidal anti-inflammatory drug
PGE_2: Prostaglandin E_2
PHCjE: Primary human cultivated conjunctival epithelial
QC: Quality control
SJS: Stevens-Johnson syndrome
SNP: Single nucleotide polymorphism
TEN: Toxic epidermal necrolysis
TLR3: Toll-like receptor 3

only environmental but also genetic factors contribute to the cause of SJS/TEN.

To elucidate the pathophysiology of SJS/TEN in more detail, in the current study we performed a genome-wide association study (GWAS) and analyzed more than 300,000 SNPs. This method permits the identification of genetic loci and genes associated with complex human traits without bias or *a priori* knowledge of the function or involvement of any gene in the disease pathway. For example, by using this strategy, our group identified SNPs in 3 different genomic loci that have modest associations with primary open-angle glaucoma.[29] In the GWAS we found 3 SNPs that were significantly associated with SJS/TEN.

Using a fine-mapping approach, we found several SNPs in the prostaglandin E receptor 3 *(EP3)* gene that were significantly associated with SJS/TEN. Supporting the genetic association of these polymorphisms with the disease, we also found that EP3 suppressed the production of cytokines induced by polyI:C stimulation and that EP3 expression was greatly reduced compared with that seen in control subjects in the conjunctival epithelium (CE) of patients with SJS/TEN, suggesting EP3 contributes functionally to the pathogenesis of SJS/TEN.

METHODS

Patients

This study was approved by the Institutional Review Board of Kyoto Prefectural University of Medicine. All experimental procedures were conducted in accordance with the principles set forth in the Declaration of Helsinki. The purpose of the research and experimental protocols was explained to all the participants, and their prior written informed consent was obtained.

The diagnoses of SJS and TEN were based on a confirmed history of acute onset of high fever, serious mucocutaneous illness with skin eruptions, and involvement of at least 2 mucosal sites, including the ocular surface. In the patients with SJS/TEN receiving a diagnosis in the acute stage at our hospital, a histological diagnosis using skin biopsy was also performed (Fig 1, *A*).[30-32] The detailed information of the patients with SJS/TEN and the control subjects who were analyzed is shown in the Methods section and Table E1 of this article's Online Repository at www.jacionline.org.

GWAS and subsequent fine-mapping of SNPs to the *EP3* region

To identify SNPs associated with SJS/TEN by means of a GWAS, we used an Affymetrix GeneChip Mapping 500K Array Set (Affymetrix, Santa Clara, Calif), according to the manufacturer's instructions (see the Methods section in this article's Online Repository).[29]

Fine-mapping analysis of the *EP3* region was performed with the iSelect Custom Infinium Genotyping system (iSelect; Illumina, Inc, San Diego, Calif), according to the manufacturer's instructions (see the Methods section in this article's Online Repository).[29]

SNP confirmation by means of direct sequencing

The 6 SJS/TEN-associated SNPs that showed significant associations ($P < .01$) in the fine-mapping analysis were confirmed by means of sequencing, as described previously (see the Methods section in this article's Online Repository).[7,24-26] The primers for both PCR and sequencing are shown in Table E2 in this article's Online Repository at www.jacionline.org. Each allele was assessed as an independent variable, and separate P values were calculated for each SNP. P values of less than .05 were regarded as statistically significant. In addition, the P values were corrected according to the number of samples tested (Bonferroni correction).

Human conjunctival tissues and primary human cultivated CE cells

For RT-PCR of the human CE, we used human CE cells obtained from healthy volunteers by means of impression cytology. The primary human cultivated conjunctival epithelial (PHCjE) cells were obtained from conjunctival tissue acquired during surgical intervention to treat conjunctivochalasis.

For immunohistochemistry, human conjunctival tissues were prepared from samples obtained during surgeries to reconstruct the ocular surface as treatment for various ocular surface diseases, including SJS and pterygium. As the control, we used the nearly normal conjunctival tissues obtained during surgery for conjunctivochalasis, a disease in which the conjunctiva relaxes because of aging, resulting in a foreign body sensation on the ocular surface.

For ELISAs, PHCjE cells were cultured as previously described (see the Methods section in this article's Online Repository at www.jacionline.org).[33]

RT-PCR

RT-PCR was performed, as previously described.[34,35] Amplification was performed with DNA polymerase (Takara, Shiga, Japan) for 40 cycles at 94°C for 1 minute, 58°C for 1 minute, and 72°C for 1 minute for human *EP3* (GeneAmp; Applied Biosystems, Foster City, Calif). The primers for human *EP3* and human glyceradlehyde-3-phosphate dehydrogenase *(GAPDH)* were, respectively: forward 5′- CGT GTA CCT GTC CAA GCA GCG TTG GGA GCA -3′ and reverse 5′- CCG TGT GTG TCT TGC AGT GCT CAA CTG ATG -3′; forward 5′- CCA TCA CCA TCT TCC AGG AG-3′ and (reverse) 5′- CCT GCT TCA CCA CCT TCT TG-3′.

Immunohistochemistry

The human conjunctival tissues were embedded in OCT compound (Sakura Finetek, Torrance, Calif) and flash-frozen in liquid nitrogen. Sections 6 μm thick were cut and fixed in 100% acetone at 4°C for 10 minutes. Immunohistochemistry was performed as previously described (see the Methods section in this article's Online Repository).[35]

ELISA

The amounts of CXCL11, CCL20, IL-6, and IL-8 released into the culture supernatant were determined by means of ELISA with the Human CXCL11, CCL20 DuoSet (R&D Systems, Inc, Minneapolis, Minn) or the OptEIATM IL-6 and IL-8 set (BD PharMingen, San Diego, Calif), respectively, according to the manufacturer's instructions.

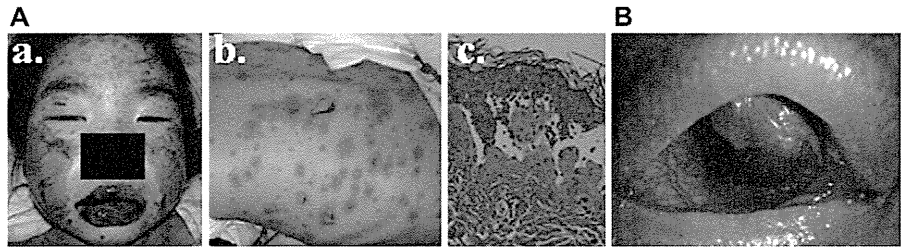

FIG 1. **A**, Skin eruptions accompanying the mucocutaneous illness of patients with SJS/TEN at the acute stage. *a*, Face with vesiculobullous lesions, conjunctivitis, and swollen crusted lips. *b*, Vesiculobullous lesions of the skin. *c*, Skin biopsy specimens of the erythematous macules showing necrotic keratinocytes and liquefaction degeneration. **B**, Ocular surface complications of patients with SJS/TEN. Conjunctival invasion results in severe vision loss.

Quantitative RT-PCR

Quantitative RT-PCR analyses for *CXCL11*, *CCL20*, and *IL6* mRNAs were performed on an ABI-prism 7700 (Applied Biosystems), as previously reported.[33-35] The primers and probes for human *CXCL11*, *CCL20*, *IL6*, and *GAPDH* were from Applied Biosystems.

Data analysis

To manage the genotype data and perform statistical analysis, we used a laboratory information management system, LaboServer (World Fusion, Tokyo, Japan). For the genotype frequency comparisons of SNPs between cases and control subjects, we used Hardy-Weinberg equilibrium analysis and the χ^2 test.

For the ELISA and quantitative RT-PCR analysis, data were expressed as mean ± SEM and were evaluated by using the Student *t* test.

RESULTS

GWAS

After genotyping 500,568 SNPs from 60 patients with SJS/TEN (cases) and 300 control subjects, we selected 313,924 SNPs using the stringent criteria chosen for our quality control (QC) filter (see the Methods section in this article's Online Repository). To identify SNPs associated with SJS/TEN, we compared the genotype frequency of each SNP between cases and control subjects. Twenty-five SNPs passed the threshold for the false discovery rate (FDR; 0.05; see Fig E1 in this article's Online Repository at www.jacionline.org). We then visually checked the 2-dimensional cluster plots of these SNPs (see the Methods section in this article's Online Repository at www.jacionline.org), and 3 of them passed our QC test (Table I). In subsequent experiments we focused on an SNP (rs17131450) that mapped close to the *EP3* gene, which is located in the 1p31 region of the human genome (Fig 2, *A*, and Table I) because the other 2 SNPs were from the "gene desert" region (see Figs E2-E5 in this article's Online Repository at www.jacionline.org).

Fine-mapping analysis of the *EP3* region

Based on the GWAS result, we performed a fine-mapping analysis of the *EP3* region using 75 cases and 448 control subjects (see Fig E6 in this article's Online Repository). We generated a custom DNA array (see the Methods section in this article's Online Repository) to analyze the SNPs in and near *EP3* through the 2 major linkage disequilibrium (LD) blocks of the HapMap Japanese (HapMap-JPT) plus HapMap Han Chinese (HapMap-CHB) populations residing within the region (Fig 2, *A*, *green bar*). We compared the genotype frequencies of 86 SNPs selected by our stringent QC filter between the cases and control subjects (see the Methods section in this article's Online Repository). The SNP (rs17131450) that showed a significant association with SJS/TEN in the GWAS also showed a significant association ($P < .01$) in the fine-mapping analysis. We also identified 5 other significantly associated ($P < .01$) SNPs in *EP3* (rs5702, rs1325949, rs7543182, rs7555874, and rs4147114; Fig 2, *A* and *C*). All of the SNPs, except rs4147114, were in Hardy-Weinberg equilibrium ($P > .05$) in the control samples. We rechecked the 2-dimensional cluster plot for rs4147114 precisely and confirmed that the distribution of the cluster was normal. One of the SNPs in *EP3* was in an exon as a silent SNP, and the other 4 were in introns (Fig 2, *C*).

TABLE I. SJS/TEN-associated SNPs obtained from the initial GWAS

SNP ID	Chromosome	SNP type	MAF	HWE in control*	Call rate†	*P* value (−log P)‡
rs1325975	6	Intergenic	0.11	0.12	0.99	5.83
rs17131450	1	Intergenic	0.09	0.11	1.00	5.77
rs11238074	11	Intergenic	0.12	0.04	0.99	5.62

**P* value for the deviation from Hardy-Weinberg equilibrium.
†Call rate per SNP in cases plus control subjects.
‡*P* value for genotype frequency comparison between cases and control subjects.

Sequencing analysis of the SJS/TEN-associated SNPs

Finally, we assessed the association of the 6 SNPs obtained from the fine-mapping analysis by sequencing samples from 100 cases and 160 control subjects. A summary of the case-control analysis based on the sequence data is shown in Table II. The association of all 6 SNPs was statistically significant, even with the Bonferroni correction ($P < .0083$). in the dominant model (Table II and Fig 2, *B*). All were in Hardy-Weinberg equilibrium ($P > .001$) in both the case and control samples. Four of the 5 SNPs in *EP3* (rs5702, rs1325949, rs7543182, and rs7555874) showed a strong LD with each other (average $D' > 0.9$, $r^2 > 0.7$; Fig 2, *B*). We identified 2 major haplotypes (types 1 and 2) of these 4 SNPs (Table III), and we also observed a significant association with SJS/TEN in various combinations of haplotypes. Consequently, from the results of the initial GWAS to those of direct sequencing, we successfully identified 6 SNPs associated with SJS/TEN, 5 of which were located within the *EP3* gene.

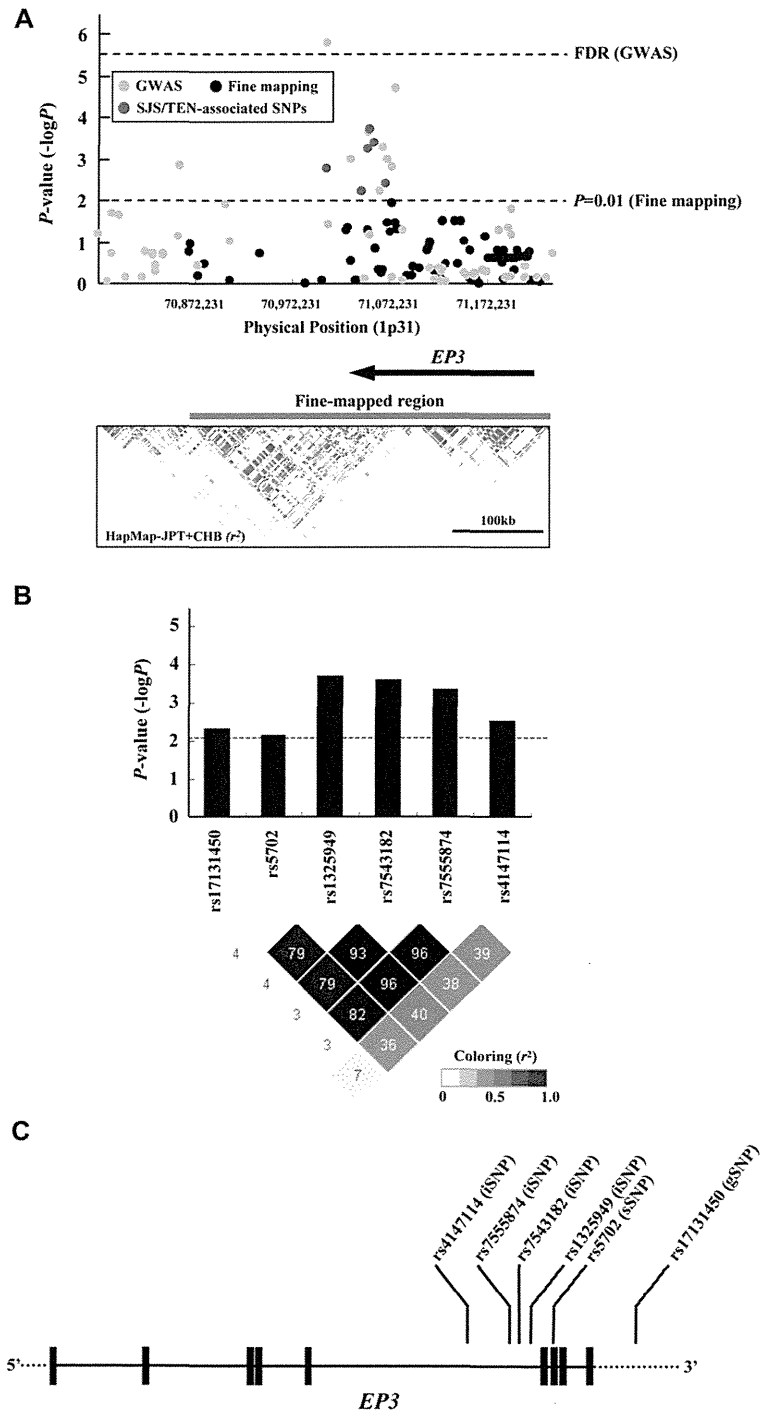

FIG 2. Association of SNPs in the *EP3* gene with SJS/TEN. **A**, Distribution of *P* values from the GWAS and fine-mapping analysis *(horizontal green bar)* of the *EP3* region. We obtained 6 significant SNPs with *P* values of less than .01 (genotype frequency comparison; *red dots*). The *P* values were plotted against the physical position of the 1p31 region and are shown for the GWAS *(gray dots)* and fine-mapping analysis *(black dots). Horizontal lines*, FDR threshold for the GWAS, which was exceeded by rs17131450 (FDR; $P = 4.0 \times 10^{-6}$, *black dotted line*), and the threshold for the fine-mapping analysis ($P = .01$, *blue dotted line*). *Horizontal arrow*, Orientation of *EP3* gene transcription. The LD block of the HapMap-JPT plus HapMap-CHB populations was obtained from the USCS Genome Browser (http://genome.ucsc.edu/; National Center for Biotechnology Information build 35). **B**, Sequencing analysis of the SNPs associated with SJS/TEN. The *P* value of a dominant model for each SNP was calculated (see also Table II). *Dotted line*, Significance threshold for the Bonferroni correction. Pairwise r^2 plots among the SNPs were generated with Haploview software (http://www.broadinstitute.org/haploview/haploview). **C**, Schematic representation of the *EP3* gene structure and the location of the SNPs associated with SJS/TEN. Note that the direction of transcription is the reverse of that shown in Fig 2, *A*.

TABLE II. Genotype frequencies and association results for SJS/TEN-associated SNPs

SNP	Position (chromosome 1)	Genotypes	Frequency of genotypes (%)		Association results		
			Control subjects (n = 160)	Patients with SJS/TEN (n = 100)	Allele 1 vs allele 2	Genotype 11 vs 12+22	Genotype 11+12 vs 22
					P value,* OR (95% CI)	*P* value,* OR (95% CI)	*P* value,* OR (95% CI)
rs17131450	71,296,002	11 CC	141 (88.1)	75 (75.0)	.00056, 0.36 (0.2-0.7)	.00600, 0.40 (0.2-0.8)	.0092, 0.10 (0.01-0.7)
		12 CT	18 (11.3)	19 (19.0)			
		22 TT	1 (0.6)	6 (6.0)			
rs5702	71,331,430	11 CC	80 (50.0)	67 (67.0)	.0300, 1.6 (1.0-2.4)	.00710, 2.0 (1.2-3.4)	.97, ND (ND)
		12 CT	67 (41.9)	25 (25.0)			
		22 TT	13 (8.1)	8 (8.0)			
rs1325949	71,337,193	11 AA	76 (47.5)	71 (71.0)	.0014, 2.0 (1.3-3.1)	.00020, 2.7 (1.6-4.6)	.61, ND (ND)
		12 AG	70 (43.8)	22 (22.0)			
		22 GG	14 (8.8)	7 (7.0)			
rs7543182	71,339,973	11 GG	80 (50.0)	73 (73.0)	.0023, 2.0 (1.3-3.1)	.00025, 2.7 (1.6-4.6)	.88, ND (ND)
		12 GT	68 (42.5)	20 (20.0)			
		22 TT	12 (7.5)	7 (7.0)			
rs7555874	71,343,960	11 GG	80 (50.0)	72 (72.0)	.0037, 1.9 (1.2-2.9)	.00046, 2.6 (1.5-4.4)	.88, ND (ND)
		12 GA	68 (42.5)	21 (21.0)			
		22 AA	12 (7.5)	7 (7.0)			
rs4147114	71,356,665	11 CC	42 (26.3)	44 (44.0)	.0033, 1.7 (1.2-2.5)	.0031, 2.2 (1.3-3.7)	.09, ND (ND)
		12 CG	82 (51.3)	42 (42.0)			
		22 GG	36 (22.5)	14 (14.0)			

ND, Not determined; OR, odds ratio.
**P* value for allele or genotype frequency comparison between cases and control subjects by using the χ^2 test.

TABLE III. Haplotypes of the SNPs in *EP3* associated with SJS/TEN

Types	SNPs				Frequency (%)	
	rs5702	rs1325949	rs7543182	rs7555874	Control subjects (n = 160)*	Patients with SJS/TEN (n = 100)*
1	C/C	A/A	G/G	G/G	46.3	67.0
2	C/T	A/G	G/T	G/A	40.0	19.0
3	T/T	G/G	T/T	A/A	7.5	7.0
4	Other combinations				6.3	8.0

*Number of subjects analyzed.

EP3 mRNA and protein expression in human ocular surface epithelium

We previously reported that EP3 is constitutively expressed in murine CE.[35] Given the association between SNPs in *EP3* and SJS/TEN and the murine expression pattern, we examined the expression of *EP3* in human CE. First, we used RT-PCR to examine the expression of *EP3* mRNA and obtained PCR products of the expected length (622 bp) from the human CE samples (Fig 3, *A, a*). PCR products were isolated and sequenced to confirm their identity. The sequences were identical to that of the human *EP3* cDNA (data not shown).

Immunohistochemistry of control human conjunctival tissue (using conjunctival tissues from a patient with conjunctivochalasis as a normal conjunctival sample) showed obvious EP3 protein expression in the CE (Fig 3, *A, b*).

Suppression of cytokine production by an EP3 agonist

We previously reported that prostaglandin E_2 (PGE_2) is a ligand for EP3 in murine CE and that it downregulates the progression of murine experimental allergic conjunctivitis.[35] We also reported that *TLR3* polymorphisms are associated with SJS/TEN in ethnic Japanese subjects,[7] that the human ocular surface epithelium expresses TLR3, and that cytokine production is upregulated by polyI:C, a TLR3 ligand.[6,34] On the basis of these findings, we examined the function of EP3 in polyI:C-stimulated PHCjE cells using an EP3 agonist, ONO-AE248. PHCjE cells that were untreated or pretreated with 10 μg/mL ONO-AE248 were incubated for 24 hours with 10 μg/mL polyI:C. As early as 24 hours after adding polyI:C, we found high levels of CXCL11, CCL20, IL-6, and IL-8 in the supernatants from the polyI:C-treated, but ONO-AE248-untreated, PHCjE cultures (Fig 3, *B, a*). Cultures pretreated with ONO-AE248 produced significantly lower levels of CXCL11, CCL20, and IL-6, but the level of IL-8 was not affected (Fig 3, *B, a*). The mRNA levels for *CXCL11*, *CCL20*, and *IL6* were also significantly less in the PHCjE cultures pretreated with ONO-AE248 compared with those seen in the untreated cultures (Fig 3, *B, b*).

Taken together, these results show that cytokine production by the CE in response to polyI:C stimulation can be suppressed through the activation of EP3.

Reduced EP3 expression in the CE of patients with SJS/TEN

Next we examined the expression of EP3 in the CE of patients with SJS/TEN by means of immunohistochemistry. Unlike in the

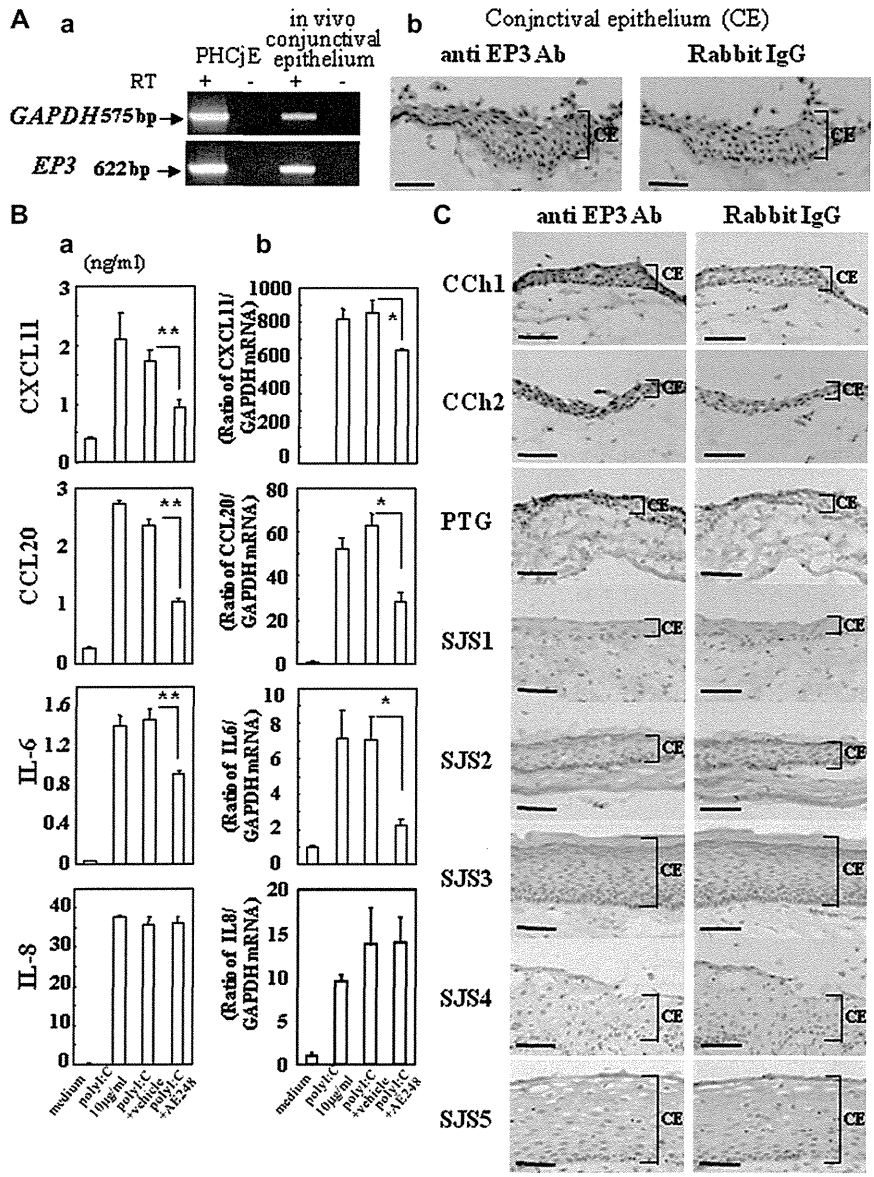

FIG 3. Expression and functional analyses of EP3 in human CE cells. **A**, *EP3* mRNA and EP3 protein expression in the human CE. *a*, RT-PCR analysis of *EP3* mRNA in normal human CE. *b*, Immunohistological analysis of EP3 in normal human conjunctival tissues. *Bars* = 50 μm. **B**, Suppression of cytokine production by an EP3 agonist. Pretreatment with ONO-AE248 significantly suppressed the protein *(a)* and mRNA *(b)* levels of CXCL11, CCL20, and IL-6 but not IL-8. Data are representative of 6 separate experiments for proteins and 2 separate experiments for mRNA. Data show the mean ± SEM from an experiment carried out in 6 wells for protein and 4 wells for mRNA per group. $*P < .05$, $**P < .01$. **C**, Reduced EP3 protein expression in the CE of patients with SJS/TEN. *CCh*, Conjunctivochalasis; *PTG*, pterygium; *SJS*, SJS/TEN. Each *bar* represents 50 μm.

control CE samples from patients with conjunctivochalasis or pterygium, we could not detect EP3 protein in the CE samples from patients with SJS/TEN (Fig 3, *C*). These results suggest that EP3, which is a receptor for PGE_2, was downregulated in the CE of patients with SJS/TEN.

DISCUSSION

In this study we performed a GWAS to identify genetic markers associated with SJS/TEN. Because of the extremely low prevalence of the disease, our GWAS was quite challenging to perform because of the sample size, which directly affects the statistical power to detect significant SNPs. As expected from the phenotype of SJS/TEN (which has been considered to be multifactorial), the low power of the study design, or both, we could not obtain genome-wide significant SNPs associated with the disease (see Fig E3 in this article's Online Repository at www.jacionline.org). However, we were able to demonstrate that as long as functional evidence could be obtained, it was worthy to perform a GWAS to list-up the candidate gene or genes or region or regions to choose and carry out follow-up functional studies. Therefore the concept of this study should shed light on future studies aimed at identifying genetic markers associated with diseases with low prevalence.

We successfully identified 3 significant SNPs in the GWAS that passed the FDR threshold, and one of them was from the *EP3* region (Fig 2, *A*). We focused on that region and discovered 5 more SNPs located in *EP3*, suggesting that *EP3* might code for a functional determinant of SJS/TEN pathogenesis (Fig 2, *A* and *C*). Further functional studies revealed that EP3 suppressed the polyI:C-induced cytokine production (Fig 3, *B*), suggesting that EP3 might function in downregulating inflammation in the CE. Indeed, EP3 protein expression in the CE was greatly reduced in patients with SJS/TEN, but it was clearly detectable in control subjects with noninflammatory ocular surface diseases (chalasis and pterygium; Fig 3, *C*). However, although significant reduction in EP3 protein expression was observed in the tissue derived from patients with SJS/TEN, the patients did not always possess the risk allele of the identified SNPs (data not shown), suggesting that EP3 levels in CE cells of the patients might be affected by not only *EP3* SNPs but also other factors, such as ocular surface inflammation. Because the SNPs in *EP3* were intronic or silent (Fig 2, *C*), they could be involved in regulating the transcription of *EP3*. Therefore we assumed that the significant reduction in EP3 expression in the CE of the patients with SJS/TEN might be due to EP3 downregulation at the transcriptional level. Such a reduction in EP3 expression in the CE of patients with SJS/TEN could contribute to ocular surface inflammation, which is a major characteristic of the disease, and therefore the polymorphisms in *EP3* might contribute to the pathophysiology of SJS/TEN.

We also found that 4 of the 6 SNPs (rs5702, rs1325949, rs7543182, and rs7555874) were in strong LD (see the Results section). According to the International HapMap project, the 6 SNPs (rs17131450, rs5702, rs1325949, rs7543182, rs7555874, and rs4147114) identified in the current study are found in both ethnic Japanese and white populations, indicating that it is important to examine these *EP3* SNPs in non-Japanese populations.

Prostanoids (ie, the prostaglandins and the thromboxanes) are a group of lipid mediators that form in response to various stimuli. They include prostaglandins D_2, E_2, $F_{2\alpha}$, and I_2 and thromboxane A_2. They are released extracellularly immediately after their synthesis, and they act by binding to a G protein–coupled rhodopsin-type receptor on the surface of target cells. Eight types of prostanoid receptors are conserved in mammals from mice to human subjects: the prostaglandin D receptor (DP), 4 subtypes of the prostaglandin E receptor (EP1, EP2, EP3, and EP4), the prostaglandin F receptor (FP), the prostaglandin I receptor (IP), and the thromboxane A receptor (TP).[36,37] PGE_2–EP3 signaling is reported to inhibit keratinocyte activation and exert anti-inflammatory actions in murine contact hypersensitivity.[38] We also previously reported that PGE_2 acts as a ligand for EP3 in the CE and downregulates the progression of murine experimental allergic conjunctivitis.[35] Here we demonstrated that an EP3 agonist suppressed the production of CXCL11, CCL20, and IL-6 by human CE cells in response to polyI:C stimulation (Fig 3, *B*). Thus EP3 in the CE might downregulate ocular surface inflammation, an idea that is supported by our finding that EP3 was strongly downregulated in the CE of patients with SJS/TEN with ocular involvement (Fig 3, *C*).

Drugs are probably the most widely accepted causative factor for SJS/TEN.[3,9,10,12] Many patients with SJS/TEN with ocular involvement have had the disease after taking remedies for the common cold or NSAIDs. Given the association between the onset of SJS/TEN and various infections, we have considered the possibility that susceptibility to SJS/TEN is related to a disordered innate immune response.[5-7,24] In this study we showed that EP3 suppressed the cytokine production elicited by stimulation with polyI:C (which mimics viral double-stranded RNA) in the human CE (Fig 3, *B*), which might suggest that EP3 is involved in innate immunity.

Of our 100 patients, 76 had SJS after being treated for the common cold with medications that included NSAIDs. NSAIDs inhibit the production of the EP3 ligand PGE_2.[39] When we analyzed the association between the 6 SNPs identified here and their frequency in the 76 cold remedy–related SJS/TEN cases, the associations remained strongly significant (data not shown). These data support the idea that EP3 is involved in the development of SJS/TEN.

In summary, we have demonstrated, using both genetic and functional analyses, that EP3 could be a key player in the pathogenesis of SJS/TEN accompanied by ocular complications.

We thank all of the patients and volunteers who enrolled in our study. We also thank Dr Natsue Omi, Ms Sayaka Ohashi, Ms Naoko Saito, and Ms Yuko Konoshima for processing blood samples and performing genotyping; Ms Hiromi Yamada for assistance in clinical information analysis; and Mr Ryuichi Sato and Ms Fumiko Sato (World Fusion, Tokyo, Japan) for management of the genotype data.

Clinical implications: EP3 could be a key player in the pathogenesis of SJS/TEN accompanied by ocular complications, and EP3 might be a target for the prevention or treatment of this disease.

REFERENCES

1. Forman R, Koren G, Shear NH. Erythema multiforme, Stevens-Johnson syndrome and toxic epidermal necrolysis in children: a review of 10 years' experience. Drug Saf 2002;25:965-72.
2. Leaute-Labreze C, Lamireau T, Chawki D, Maleville J, Taieb A. Diagnosis, classification, and management of erythema multiforme and Stevens-Johnson syndrome. Arch Dis Child 2000;83:347-52.
3. Roujeau JC, Kelly JP, Naldi L, Rzany B, Stern RS, Anderson T, et al. Medication use and the risk of Stevens-Johnson syndrome or toxic epidermal necrolysis. N Engl J Med 1995;333:1600-7.
4. Sotozono C, Ueta M, Koizumi N, Inatomi T, Shirakata Y, Ikezawa Z, et al. Diagnosis and treatment of Stevens-Johnson syndrome and toxic epidermal necrolysis with ocular complications. Ophthalmology 2009;116:685-90.
5. Ueta M. Innate immunity of the ocular surface and ocular surface inflammatory disorders. Cornea 2008;27(suppl):S31-40.
6. Ueta M, Kinoshita S. Innate immunity of the ocular surface. Brain Res Bull 2010; 81:219-28.
7. Ueta M, Sotozono C, Inatomi T, Kojima K, Tashiro K, Hamuro J, et al. Toll-like receptor 3 gene polymorphisms in Japanese patients with Stevens-Johnson syndrome. Br J Ophthalmol 2007;91:962-5.
8. Yetiv JZ, Bianchine JR, Owen JA Jr. Etiologic factors of the Stevens-Johnson syndrome. South Med J 1980;73:599-602.
9. Halevy S, Ghislain PD, Mockenhaupt M, Fagot JP, Bouwes Bavinck JN, Sidoroff A, et al. Allopurinol is the most common cause of Stevens-Johnson syndrome and toxic epidermal necrolysis in Europe and Israel. J Am Acad Dermatol 2008;58:25-32.
10. Levi N, Bastuji-Garin S, Mockenhaupt M, Roujeau JC, Flahault A, Kelly JP, et al. Medications as risk factors of Stevens-Johnson syndrome and toxic epidermal necrolysis in children: a pooled analysis. Pediatrics 2009;123:e297-304.
11. Power WJ, Ghoraishi M, Merayo-Lloves J, Neves RA, Foster CS. Analysis of the acute ophthalmic manifestations of the erythema multiforme/Stevens-Johnson syndrome/toxic epidermal necrolysis disease spectrum. Ophthalmology 1995; 102:1669-76.
12. Wolf R, Orion E, Marcos B, Matz H. Life-threatening acute adverse cutaneous drug reactions. Clin Dermatol 2005;23:171-81.
13. Chung WH, Hung SI, Hong HS, Hsih MS, Yang LC, Ho HC, et al. Medical genetics: a marker for Stevens-Johnson syndrome. Nature 2004;428:486.